Title: Paleoenvironmental change recorded in submarine fans: the Eocene-Oligocene climate transition in the Alpine foreland basin

Authors: Euan L. Soutter[1*] Ian A. Kane[1], Ander Martínez-Doñate[1], Adrian J. Boyce[2], Jack Stacey[1] and Sébastien Castelltort[3]

Institutions:

[1*]Department of Earth and Environmental Sciences, University of Manchester, Manchester, U.K.

[2]Scottish Universities Environmental Research Centre, East Kilbride, U.K.

[3]Department of Earth Sciences, University of Geneva, Geneva, Switzerland.

Email: euan.soutter@manchester.ac.uk

ABSTRACT

The Eocene-Oligocene transition (EOT) was a period of considerable environmental change, signifying the transition from Paleocene greenhouse to Oligocene icehouse conditions. Preservation of the sedimentary signal of such an environmental change is most likely in net-depositional environments, such as submarine fans, which are the terminal parts of sedimentary systems. Here, using sedimentary and stable isotope data from the Alpine foreland basin, we assess whether this major climatic transition influenced the stratigraphic evolution of submarine fans. Results indicate that fine-grained deposition in deep-water environments corresponds to positive $\delta^{13}C$ excursions and eustatic highstands, while coarse-grained deposition corresponds to negative $\delta^{13}C$ excursions and eustatic lowstands during the earliest Oligocene. These results indicate that: 1) eustatic sea-level plays a major role in dictating sediment supply to deep-water in foreland basins and, 2) sea-level fluctuations related to Antarctic icesheet growth across the Eocene-Oligocene transition influenced sediment supply to deep-water environments.

INTRODUCTION

The stratigraphic record of major environmental change is expected to be best recorded in net-depositional environments, such as submarine fans (e.g. Hessler and Fildani, 2019). Submarine fans are built from the deposits of sediment-gravity flows that transport vast quantities of terrigenous sediment and organic carbon to deep-marine environments (e.g. Galy et al. 2007). Submarine fan growth has been shown to occur during both low and high eustatic sea levels (e.g. Covault et al. 2011) and may be driven by a combination of tectonic events (e.g. Howarth et al. 2021) and onshore climate change (e.g. Picot et al. 2019), all of which can be overprinted by autogenic processes. Disentangling allogenic from autogenic influences on submarine fan deposition has therefore proven to be difficult (Ferguson et al. 2020), with allogenic signals often attenuated within the sediment routing system (Romans et al. 2016). Measurement of $\delta^{13}C$ in exhumed stratigraphy has been used as a means of addressing this problem, with $\delta^{13}C$ sensitive to many of the environmental factors that influence submarine fan deposition (e.g. Castelltort et al. 2017). Positive $\delta^{13}C$ excursions are considered to correspond to high sea-levels, flooded continental shelves, high biological productivity and burial of ^{12}C, while low $\delta^{13}C$ values correspond to low-sea levels, exposed shelves, lower productivity and greater run-off (Jenkyns, 1993; Castelltort et al. 2017). By constructing a $\delta^{13}C$ curve through a deep-marine sequence of a known age it is therefore possible to relate sedimentation to eustatic and climatic trends (Castelltort et al. 2017).

The Eocene-Oligocene climate transition (EOT) between ~34 and ~33 Ma was a major environmental response to the opening of oceanic gateways in the Southern Oceans (Kennett, 1977), decreased atmospheric CO_2 (Pearson et al. 2009) and orbital forcing (Ladant et al. 2014), and resulted in the establishment of major Antarctic ice sheets (Liu et al. 2009), and the transition from Paleogene greenhouse to current icehouse conditions (Wade et al. 2012). The EOT occurred through a series of global cooling 'steps' that correspond to positive $\delta^{18}O$ excursions, such as the 'Oi-1' event at ~33.55 ma, which represents a major eustatic sea-level fall related to Antarctic ice sheet growth (Katz et al. 2008).

The Grès d'Annot Formation is an exhumed siliciclastic deep-marine succession that was deposited within the Alpine foreland basin during the EOT (Fig. 1A, 1B; Fig. 2) (Joseph and Lomas, 2004). The Grès d'Annot records a common deep-marine stratigraphic pattern of fine-grained intervals interspersed with coarser-grained intervals, with each > 10 m thick interval composed of numerous individual event beds. This apparent cyclicity has been attributed to sea-level change and tectonism (Fig. 2) (Callec, 2004, Euzen et al. 2004); however, the relative impact of these controls has not been tested. This study therefore aims to investigate, through high-resolution isotopic analysis of the Grès d'Annot stratigraphy, whether: 1) the EOT and associated eustatic and climatic change is resolved in the Grès d'Annot isotopic record, and 2) whether this environmental change affected submarine fan deposition in the Alpine foreland basin. On a broader scale, this study aims to explore how the isotopic records of exhumed submarine fans can be used to understand how past landscapes responded to environmental change.

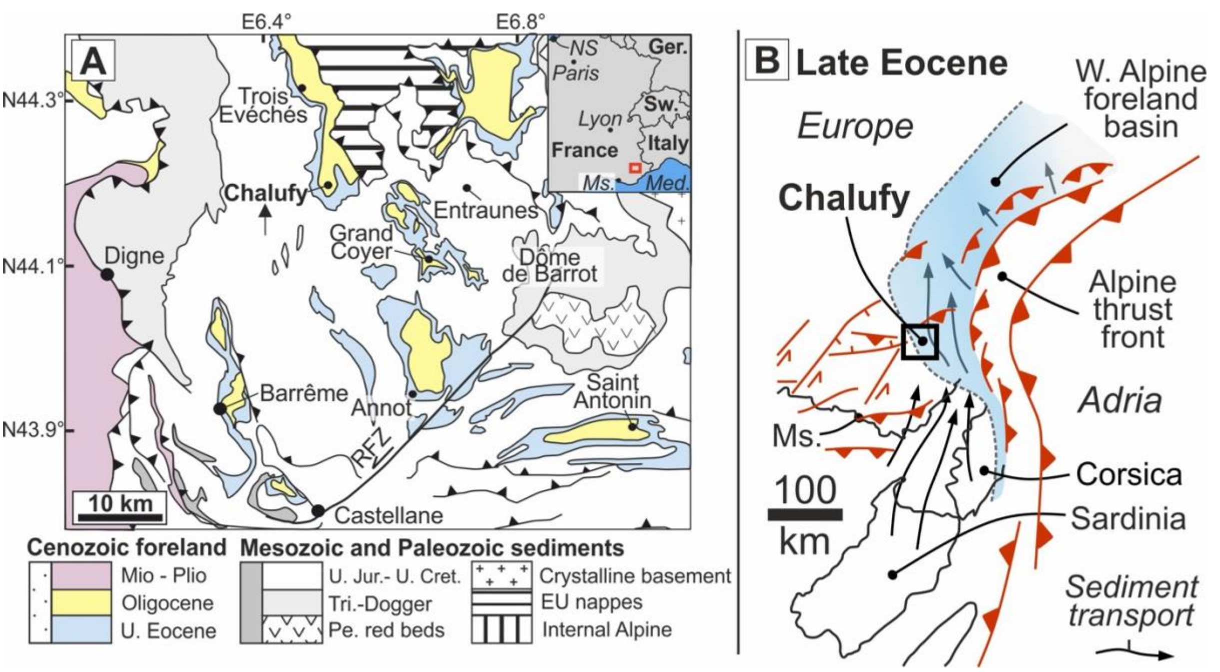

STUDY AREA: CHALUFY

One of the most well-studied Grès d'Annot exposures is located at the Montagne de Chalufy (Fig. 1A; B), representing a relatively distal part of the Grès d'Annot submarine fan system (Du Fornel et al. 2004) (Fig. 1A; Fig. 2B). The exposure comprises three coarse-grained sandstone intervals deposited sequentially against a marl paleo-slope (Puigdefabregas et al. 2004) (Fig. S1). The coarse-grained intervals are interpreted as the deposits of high-concentration turbidity currents that built submarine fan lobes on the basin floor. These coarse-grained intervals alternate with finer-grained mudstone and siltstone intervals, which are interpreted as the deposits of lower-concentration turbidity currents, interbedded with thin hemipelagic mudstones deposited at the distal extents of the coarse-grained lobes or distributary channels on the basin floor (Fig. 2; Fig. S1).

Identification of foraminifera belonging to known planktonic (P) and nano-planktonic (NP) biozones indicates that the basal part of the Grès d'Annot exposed at Chalufy was deposited at a maximum of 34.2 Ma (NP20/NP21), with the uppermost parts of the Grès d'Annot being deposited at 32.8 Ma (NP21/22) or a minimum of 32 Ma (top P18) (Fig. 2A) (Euzen et al. 2004; Du Fornel et al. 2004). The base of P17 occurs prior to the first coarse-grained interval (Fig. 2A) (Du Fornel et al. 2004). For consistency with the existing Alpine foreland chronostratigraphic framework, and other isotopic and eustatic datasets used, all ages are tied to the chronology of Berggren et al. (1995).

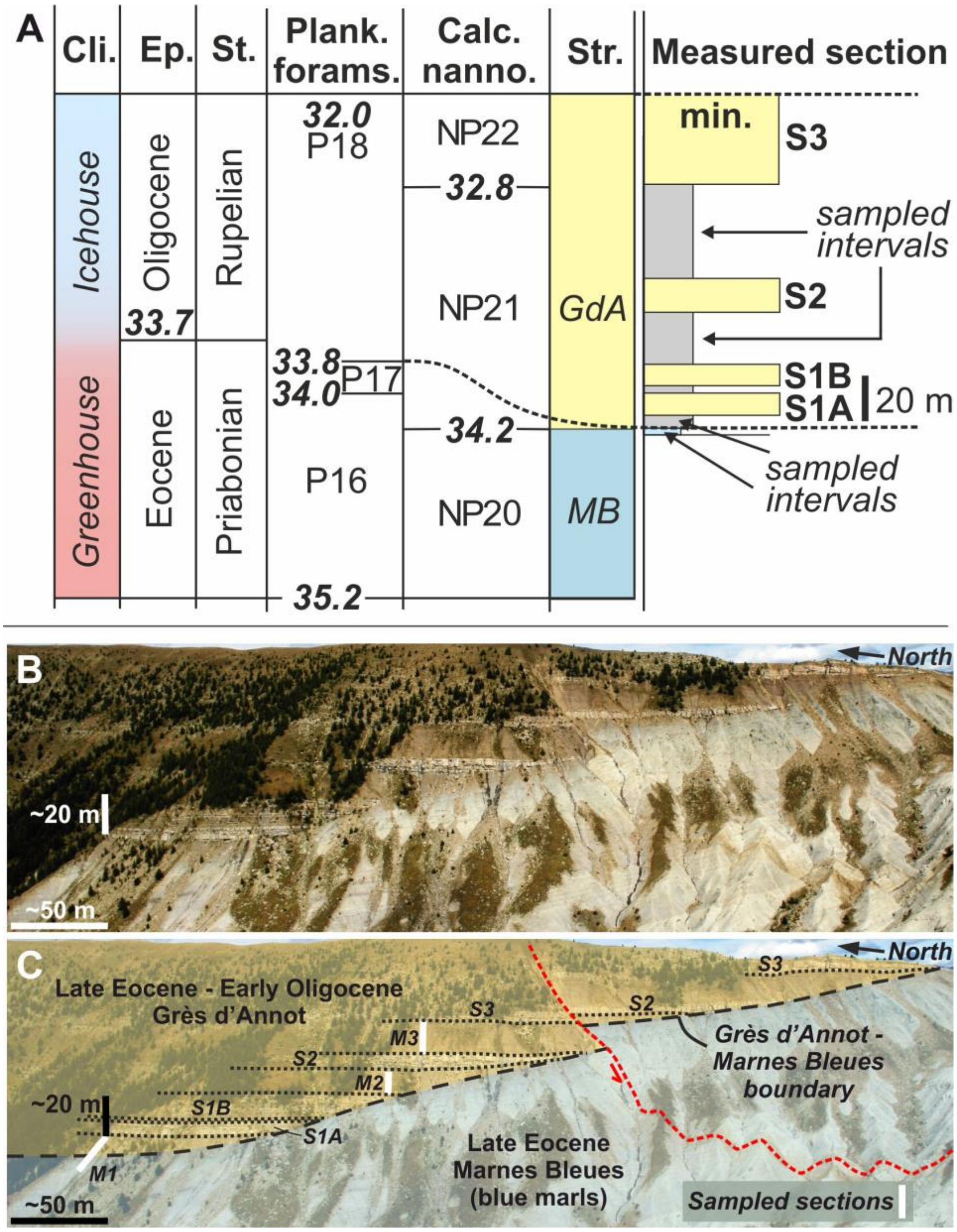

DATA AND METHODS

111 samples were recovered from three fine-grained intervals in one continuous measured section (~148 m) spanning the Grès d'Annot exposure at the Chalufy paleo-slope (Fig. 3; Fig. 2, S1; S2; Table S1). The samples were collected at ~60 cm intervals, from > 30 cm below the exposed surface and only within hemipelagic sections, thus avoiding potential contamination by allochthonous material. The samples were crushed and their bulk carbonate $\delta^{13}C$ and $\delta^{18}O$ values measured using standard techniques (Brodie et al. 2018), with 9 repeated measurements of section-

representative samples yielding a mean measurement error of ± 0.3 for $\delta^{13}C$ and ± 0.1 for $\delta^{18}O$ (Fig. 3; S2). Carbon and oxygen isotopes are reported per mil (‰) relative to the Vienna Pee Dee Belemnite Standard (VPDB) (Fig. S2).

Three isotopic curves representing each fine-grained interval were generated through the application of a Savitzky–Golay filter to the individual data points, which smooths the data without distorting the underlying signal (Fig. 3; S2; S3) (Savitzky and Golay, 1964). The data were iteratively smoothed through various window-lengths until a dominant signal emerged (Fig. S7). These curves were then placed within bounding-age constraints derived from micropaleontological zonation of the study area (Du Fornel et al. 2004) and assessed for correlation with the time-equivalent global $\delta^{13}C$ curve (Cramer et al. 2009) and the North Atlantic eustatic sea-level curve (Miller et al. 2005). Randomly selected samples have also undergone X-ray diffraction (XRD), total organic carbon (TOC) (Table S1) and petrographic analysis (Fig. S6) in order to assess the potential for mixed-carbonate-source error or diagenetic overprinting.

RESULTS

The bulk $\delta^{13}C$ content was measured from 111 samples (Fig. 3; Fig. S1). The identification of benthic foraminifera during petrographic analysis of the samples (Fig. S6) and the occurrence of dateable benthic foraminifera within the Chalufy section (Fig. 2A) indicates that the bulk $\delta^{13}C$ measurements primarily record the signature of this fauna. The observed depletion in $\delta^{18}O$ values suggests some diagenetic influence, which may have also impacted the $\delta^{13}C$ values. Cross-plotting of $\delta^{13}C$ and $\delta^{18}O$ from each interval also shows no statistically-significant trends, suggesting a lack of diagenetic overprinting (Marshall, 1991) (Fig. S5). X-ray diffraction of selected samples within each interval indicates total organic carbon (TOC) contents of < 0.7 % and calcite to organic matter ratio of > 7:1, indicating that the likelihood of diagenetic contamination from organic carbon is low (Saltzmann and Thomas, 2012).

The $\delta^{13}C$ data shows a broadly increasing spread with increasing height in the section ($1\sigma = 0.5$ ‰, 0.4 ‰, 0.9 ‰, 1.0 ‰ for each sequential fine-grained interval) (Fig. S4), with mean $\delta^{13}C$ values being 2.0 ‰ more negative than time-equivalent open oceanic values (Cramer et al., 2009). Data noise and more negative $\delta^{13}C$ values are attributed to: 1) the relatively proximal position of the basin resulting in the oxidation of light organic ^{12}C delivered by rivers (Jenkyns, 1996; Voigt and Hilbrecht, 1997), and 2) microscopic turbidites or authigenic carbonate, such as micro-veins, within the hemipelagic sections creating allochthonous noise (Fig. S7; S6). These unavoidable diagenetic and environmental factors potentially acted to adjust the isotopic values, likely precluding accurate high-resolution cyclo-stratigraphy (e.g. precessional trends). Lower-resolution isotopic trends (e.g. eccentric trends) are suggested to be resolved, however, as a result of the high sampling density and resultant smoothed curves.

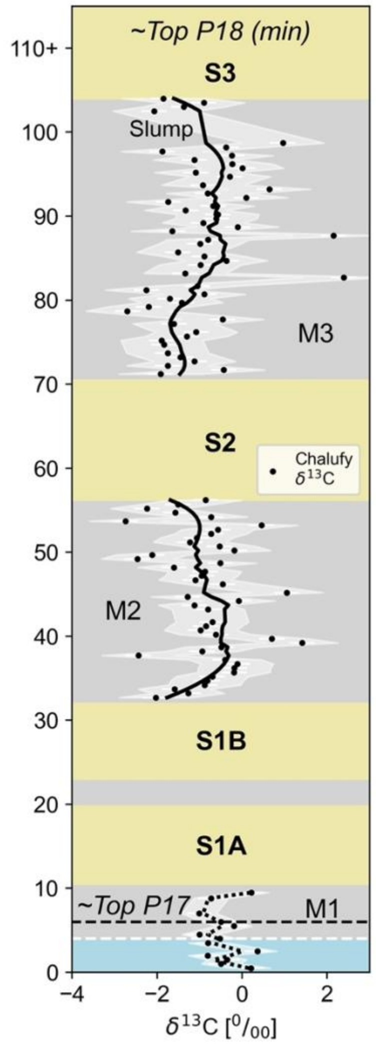

The $\delta^{13}C$ curves of Mudstone 2 (M2) and Mudstone 3 (M3) (sandstone-bounded fine-grained intervals) each show a general trend of increasing then decreasing $\delta^{13}C$ values with increasing height (Fig. 3). Within the micropalaeontological constraints these curves could be correlated to similar excursions in the smoothed global $\delta^{13}C$ curve between 33.5 and 33.0 Ma, or between two rising then falling sections of the global eustatic curve between 33.5 and 32.3 Ma (Fig. 4). Due to the restricted nature of the Alpine foreland basin (Fig. 1B), which would have prevented rapid exchange with the global carbon reservoir (Saltzmann and Thomas, 2012), and the relatively proximal position of the sampled stratigraphy (Fig. 1B), the eustatic correlation is most probable (e.g. Castelltort et al. 2017). M2 and M3 therefore correlate with eustatic sea-level highstands, with the sandstones at ends of the curves (S1B, S2 and S3) correlating with sea-level lowstands (Fig. 4).

There is uncertainty in how much time is occupied between the upper marl surface and Grès d'Annot deposition as the older part of the stratigraphy was not deposited at the sampled location, which is higher on the basin margin slope (Du Fornel et al. 2004). Accordingly, the isotopic trends within the lowermost sections cannot be confidently interpreted.

The Chalufy $\delta^{18}O$ values show a generally decreasing, but noisy, trend in M2, and a sharply increasing then sharply decreasing trend in M3. However, due to diagenesis, these $\delta^{18}O$ trends are expected to be less reliable than the $\delta^{13}C$ trends and are consequently not used as a basis for interpretation (Fig. S2).

DISCUSSION

The observed correlation between submarine fan retreat and global positive $\delta^{13}C$ excursions indicates that; 1) the isotopic record of the Chalufy section resolves cycles of environmental change across the EOT and in the early Oligocene, and 2) deposition in the Alpine foreland was influenced by the environmental factors driving these excursions. The correlation between the positive $\delta^{13}C$ excursions and time-equivalent global eustatic highstands indicates that sea-level change drove these excursions. Fine-grained deposition in the deep-water foreland basin is therefore linked to high sea-levels, while coarse-grained deposition is linked to low sea-levels. These results are consistent with those made in the Eocene Pyrenean foreland basin (Castelltort et al. 2017), with positive $\delta^{13}C$ excursions found to correlate with eustatic sea-level highstands and reduced sediment supply to submarine fans. Low sea-levels tend to enhance siliciclastic deep-marine deposition as rivers are able to deliver sediment directly to the shelf-edge and deeper waters. In the Quaternary Golo Fan this process has been invoked to explain widespread fine-grained deposition in submarine fans during interglacial highstands and coarser-grained deposition during glacial lowstands (Sweet et al. 2020). These results suggest an analogous control on sediment supply to deep-water in the Paleogene Alpine foreland basin.

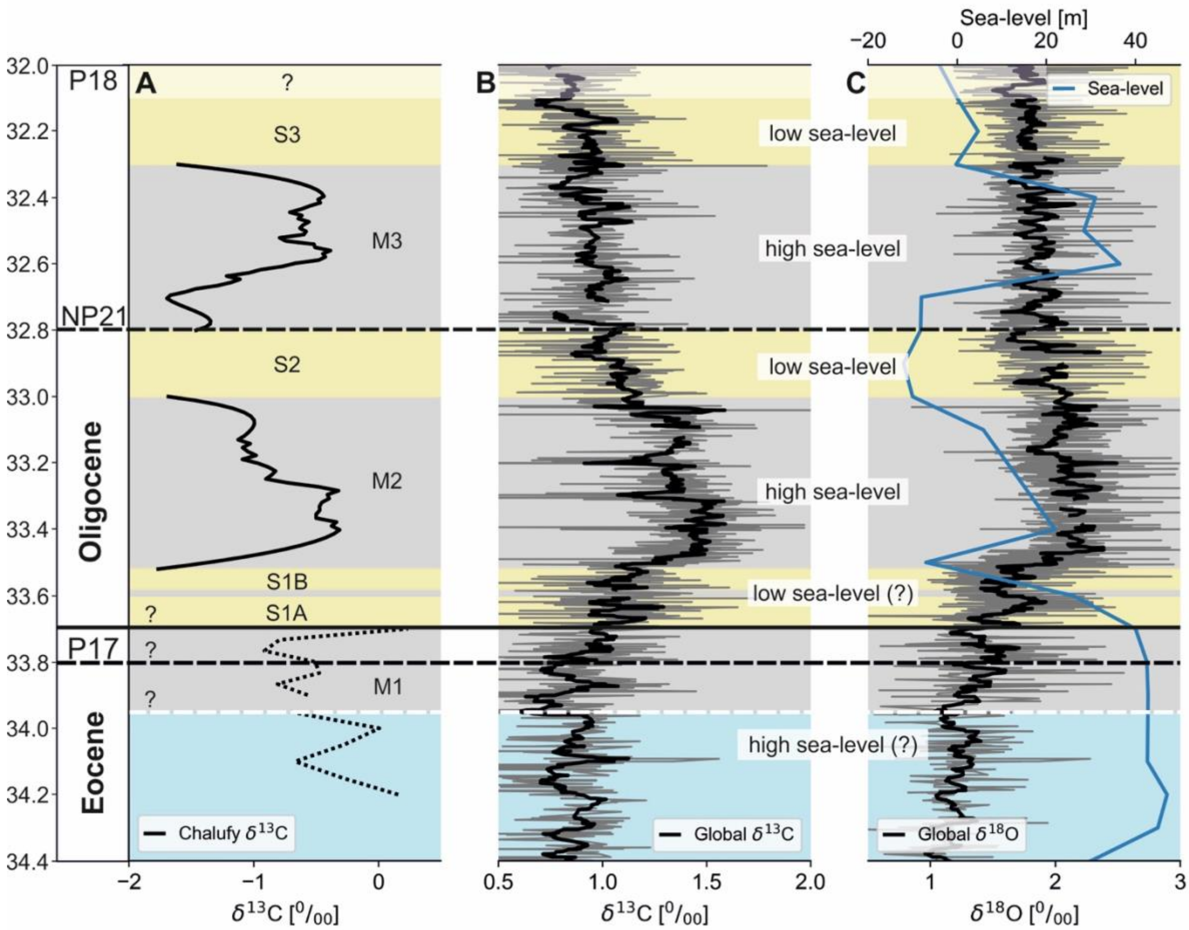

Sea-level fluctuations during the early Oligocene are likely driven by fluctuations in volume of the newly-established Antarctica ice sheet (Katz et al. 2008), with the positive $\delta^{13}C$ excursions identified here likely representing periods of warmer periods and decreased ice sheet volume. This may indicate that onshore climate change across the Eocene-Oligocene transition also influenced deposition in the Alpine foreland. Warmer climates act to reduce sediment supply to submarine fans by expanding vegetation cover and trapping sediment in catchments, as observed during warm Pleistocene interglacials in the Gulf of Corinth (Cullen et al. 2021). Conversely, cooler climates may increase sediment supply to submarine fans through increased continental weathering, as invoked to explain increased terrigenous sediment supply to marine environments offshore western Africa during early Oligocene cooling (Séranne, 1999). Similar climatic mechanisms may have operated in tandem with eustasy to modulate coarse-grained sediment supply to the deep-water Alpine foreland during the early Oligocene. This may be indirectly reflected in the $\delta^{13}C$ record of the fine-grained sections, with a reduction in the volume of ^{12}C transported to marine environments by rivers consistent with the observed positive $\delta^{13}C$ excursions (Voigt and Hilbrecht, 1997).

CONCLUSION

Submarine fan evolution is intimately linked to tectonic and climatic processes. The stratigraphic record of submarine fans is therefore expected to archive major tectonic and climatic events. Here we show that positive $\delta^{13}C$ excursions correspond to periods of reduced sediment delivery to the Alpine foreland basin. These positive $\delta^{13}C$ excursions are linked to periods of eustatic highstand across the Eocene-Oligocene transition that decreased sediment supply to deep-water environments. Expansion of vegetation during these warmer periods may have also acted to reduce sediment supply to deep-water. Sea-level lowstands driven by icesheet expansion resulted in increased sediment supply to submarine fans and coarse-grained deposition in the basin. This study indicates that the coupled influence of sea-level and onshore climate change across the EOT and during the early Oligocene affected submarine fan deposition in Alpine foreland, further highlighting the utility of exhumed submarine fans as archives of environmental change.

ACKNOWLEDGEMENTS

Soutter is funded by NERC grant number NE/M00578X/1. We thank three anonymous reviewers for their detailed comments and suggestions on an earlier version of the manuscript, which greatly improved the manuscript. We wish to thank Julie Dougans (SUERC) for technical assistance in the stable isotope analyses.

FIGURE CAPTIONS

Figure 1: A) Geological map of the Alpine foreland and the location of the sampled section at Montagne de Chalufy (black arrow). Inset is present-day European location. Red box is geological map area. Black lines with teeth represent thrust faults, with teeth on hangingwall. (modified from Joseph and Lomas, 2004). U. = upper; Mio-Plio = Miocene-Pliocene; Jur. = Jurassic; Cret. = Cretaceous, Tri. = Triassic; Pe = Permian. EU = Embrunais-Ubaye. B) Palinspastic reconstruction and paleogeographic setting of the Alpine foreland basin during the Late Eocene (modified from Dumont et al. 2011). Ms = Marseille; NS = North Sea; Sw. = Switzerland; Ger. = Germany; Med. = Mediterranean.

Figure 2: A) Chronostratigraphic framework of the studied section (modified from Euzen et al., 2004). The base of P18 is precedes deposition of S1A. Micropaleontological zonation (NP & P zones) of the studied stratigraphy (modified from Euzen et al. 2004). Eocene – Oligocene boundary shifted to that of Katz et al. (2008). B) Uninterpreted and interpreted (C) sampled sections at Chalufy and stratigraphic context. Red dashed line indicates a fault. Grid reference: 44°09'21''N, 6°32'51E. GdA = Gres d'Annot; MB = Marnes Bleues; Cli. = generalized climate; Ep. = epoch; St. = stage, Plank. forams = planktonic foraminifera; Calc. nano. = calcareous nannofossils; Strat: stratigraphy; P: planktonic; NP: nanoplanktonic; S = sandstone; M = mudstone.

Figure 3: δ^{13}C measurements for each fine-grained interval sampled and their bounding P-Zones (planktonic zones) (Du Fornel et al. 2004). The black solid line represents a Savitzky-Golay filter. Yellow = sandstone, grey = mudstone and siltstone, blue = marl. The white line is an uncertain age break. Error bar is the mean error of δ^{13}C standards. Light grey envelope is one standard deviation.

Figure 4: Correlation of A) the δ^{13}C record from Chalufy, B) Global δ^{13}C curve (Cramer et al. 2008), and C) Global δ^{18}O curve and North Atlantic sea-level (Miller et al. 2005). C-S = Corsica-Sardinia, yellow = sandstone, grey = mudstone and siltstone, blue = marl. Ages tied to the chronology of (Bergrenn et al. 1995; Cande and Kent, 1995). The white line indicates uncertain age break. Solid black lines are Savitzky–Golay filtered data, grey lines indicate raw data.

REFERENCES

Berggren, W. A., Kent, D. V., Swisher, C. C. & Aubry, M.-P, 1995, Geochronology, Time Scales and Global Stratigraphic Correlations: A Unified Temporal Framework for an Historical Geology, eds Berggren, W. A., Kent, D. V. & Hardenbol, J.: SEPM, p. 129–212.

Brodie, M.W., Aplin, A.C., Hart, B., Orland, I.J., Valley, J.W. and Boyce, A.J., 2018, Oxygen isotope microanalysis by secondary ion mass spectrometry suggests continuous 300-million-year history of calcite cementation and dolomitization in the Devonian Bakken Formation: Journal of Sedimentary Research, v. 88, 91-104.

Cande, S.C. and Kent, D.V., 1995, Revised calibration of the geomagnetic polarity timescale for the Late Cretaceous and Cenozoic: Journal of Geophysical Research: Solid Earth, v. 100, p. 6093-6095.

Castelltort, S., Honegger, L., Adatte, T., Clark, J.D., Puigdefàbregas, C., Spangenberg, J.E., Dykstra, M.L. and Fildani, A., 2017, Detecting eustatic and tectonic signals with carbon isotopes in deep-marine strata, Eocene Ainsa Basin, Spanish Pyrenees: Geology, v. 45, p. 707-710.

Covault, J.A., Romans, B.W., Graham, S.A., Fildani, A. and Hilley, G.E., 2011, Terrestrial source to deep-sea sink sediment budgets at high and low sea levels: Insights from tectonically active Southern California: Geology, v. 39, p. 619-622.

Cramer, B.S., Toggweiler, J.R., Wright, J.D., Katz, M.E. and Miller, K.G., 2009. Ocean overturning since the Late Cretaceous: Inferences from a new benthic foraminiferal isotope compilation: Paleoceanography, v. 24.

Cullen, T.M., Collier, R.E.L., Hodgson, D.M., Gawthorpe, R., Kouli, K., Maffione, M., Kranis, H. and Eliassen, G.T., 2021, Deep-water syn-rift stratigraphy as archives of Early-Mid Pleistocene palaeoenvironmental signals and controls on sediment delivery: EarthArXiv, https://doi.org/10.31223/X58892

Du Fornel, E., Joseph, P., Desaubliaux, G., Eschard, R., Guillocheau, F., Lerat, O., Muller, C., Ravenne, C. and Sztrakos, K., 2004, The southern Grès d'Annot outcrops (French Alps): an attempt at regional correlation: Geological Society, London, Special Publications, v. 221, p. 137-160.

Ducassou, E., Migeon, S., Mulder, T., Murat, A., Capotondi, L., Bernasconi, S.M. and Mascle, J., 2009. Evolution of the Nile deep-sea turbidite system during the Late Quaternary: influence of climate change on fan sedimentation: Sedimentology, v. 56, p. 2061-2090.

Dumont, T., Simon-Labric, T., Authemayou, C. and Heymes, T., 2011. Lateral termination of the north-directed Alpine orogeny and onset of westward escape in the Western Alpine arc: Structural and sedimentary evidence from the external zone: Tectonics, v. 30.

Euzen, T., Joseph, P., Du Fornel, E., Lesur, S., Granjeon, D. and Guillocheau, F., 2004. Three-dimensional stratigraphic modelling of the Grès d'Annot system, Eocene-Oligocene, SE France. Geological Society, London, Special Publications, v. 221, p. 161-180.

Ferguson, R., Kane, I.A., Eggenhuisen, J., Pohl, F., Tilston, M., Spychala, Y. and Brunt, R., 2020, Entangled external and internal controls on submarine fan evolution: an experimental perspective: The Depositional Record.

Galy, V., France-Lanord, C., Beyssac, O., Faure, P., Kudrass, H. and Palhol, F., 2007, Efficient organic carbon burial in the Bengal fan sustained by the Himalayan erosional system: Nature, v. 450, p. 407-410.

Hessler, A.M. and Fildani, A., 2019. Deep-sea fans: tapping into Earth's changing landscapes: Journal of Sedimentary Research, v. 89, p. 1171-1179.

Howarth, J.D., Orpin, A.R., Kaneko, Y. et al. 2021. Calibrating the marine turbidite palaeoseismometer using the 2016 Kaikōura earthquake: Nature Geoscience. In press.

Jenkyns, H.C., 1996, Relative sea-level change and carbon isotopes: Data from the upper Jurassic (Oxfordian) of central and Southern Europe: Terra Nova, v. 8, p. 75-85.

Joseph, P. and Lomas, S.A., 2004, Deep-water sedimentation in the Alpine Foreland Basin of SE France: New perspectives on the Grès d'Annot and related systems—an introduction: Geological Society, London, Special Publications, v. 221, p. 1-16.

Katz, M.E., Miller, K.G., Wright, J.D., Wade, B.S., Browning, J.V., Cramer, B.S. and Rosenthal, Y., 2008, Stepwise transition from the Eocene greenhouse to the Oligocene icehouse: Nature Geoscience, v. 1, p. 329.

Kennett, J.P., 1977, Cenozoic evolution of Antarctic glaciation, the circum-Antarctic Ocean, and their impact on global paleoceanography: Journal of Geophysical Research, v. 82, p. 3843-3860.

Ladant, J.B., Donnadieu, Y., Lefebvre, V. and Dumas, C., 2014, The respective role of atmospheric carbon dioxide and orbital parameters on ice sheet evolution at the Eocene-Oligocene transition: Paleoceanography, v. 29, p. 810-823.

Liu, Z., Pagani, M., Zinniker, D., DeConto, R., Huber, M., Brinkhuis, H., Shah, S.R., Leckie, R.M. and Pearson, A., 2009, Global cooling during the Eocene-Oligocene climate transition: Science, v. 323, p. 1187-1190.

Marshall, J.D., 1991, Climatic and oceanographic isotopic signals from the carbonate rock record and their preservation: Geological magazine, v. 129, p. 143-160.

Miller, K.G., Kominz, M.A., Browning, J.V., Wright, J.D., Mountain, G.S., Katz, M.E., Sugarman, P.J., Cramer, B.S., Christie-Blick, N. and Pekar, S.F., 2005, The Phanerozoic record of global sea-level change: Science, v. 310, p. 1293-1298.

Pearson, P.N., Foster, G.L. and Wade, B.S., 2009, Atmospheric carbon dioxide through the Eocene–Oligocene climate transition: Nature, v. 461, p. 1110.

Picot, M., Marsset, T., Droz, L., Dennielou, B., Baudin, F., Hermoso, M., De Rafélis, M., Sionneau, T., Cremer, M., Laurent, D. and Bez, M., 2019, Monsoon control on channel avulsions in the Late Quaternary Congo Fan: Quaternary Science Reviews, v. 204, p. 149-171.

Puigdefàbregas, C., Gjelberg, J. and Vaksdal, M., 2004, The Grès d'Annot in the Annot syncline: outer basin-margin onlap and associated soft-sediment deformation: Geological Society, London, Special Publications, v. 221, p. 367-388.

Romans, B.W., Castelltort, S., Covault, J.A., Fildani, A. and Walsh, J.P., 2016, Environmental signal propagation in sedimentary systems across timescales: Earth-Science Reviews, v. 153, p. 7-29.

Saltzman, M.R., and Thomas, E., 2012, Carbon isotope stratigraphy, in Gradstein, F., et al., eds., The geologic time scale: Oxford, UK, Elsevier, p. 207–232.

Savitzky and M. J. E. Golay, 1964, Soothing and differentiation of data by simplified least squares procedures: Anal. Chem., v. 36, p. 1627-1639.

Voigt, S. and Hilbrecht, H., 1997, Late Cretaceous carbon isotope stratigraphy in Europe: correlation and relations with sea level and sediment stability: Palaeogeography, Palaeoclimatology, Palaeoecology, v. 134, p. 39-59.

Séranne, M., 1999, Early Oligocene stratigraphic turnover on the west Africa continental margin: a signature of the Tertiary greenhouse-to-icehouse transition?: Terra Nova-Oxford, v. 11, p. 135-140.

Sweet, M.L., Gaillot, G.T., Jouet, G., Rittenour, T.M., Toucanne, S., Marsset, T. and Blum, M.D., 2020, Sediment routing from shelf to basin floor in the Quaternary Golo System of Eastern Corsica, France, western Mediterranean Sea: GSA Bulletin, v. 132, p.1217-1234.

Zachos, J.C. and Kump, L.R., 2005, Carbon cycle feedbacks and the initiation of Antarctic glaciation in the earliest Oligocene: Global and Planetary Change, v. 47, p. 51-66.

SUPPLEMENTARY CAPTIONS

Figure S1: Logged section at Chalufy and sample locations. Middle and upper sandstones from Puigdefabregas et al. (2004). Numbers refer to sand unit described in text.

Figure S2: $\delta^{13}C$ and $\delta^{18}O$ measurements for each fine-grained interval sampled and their bounding P Zones (Du Fornel et al. 2004). Yellow = sandstone, grey = mudstone and siltstone, blue = marl. The white line is an uncertain age break. Error bar is the mean error of $\delta^{13}C$ and $\delta^{18}O$ standards (mean error assigned to each data point). Light grey envelope is one standard deviation of each fine-grained grained interval.

Figure S3: Correlation between A) the $\delta^{13}C$ record of Chalufy, B) Global $\delta^{13}C$ curve (Cramer et al. 2008), C) the $\delta^{18}O$ record of Chalufy, and D) Global $\delta^{18}O$ curve and North Atlantic sea-level (Miller et al. 2005). C-S = Corsica-Sardinia, yellow = sandstone, grey = mudstone and siltstone, blue = marl. Ages tied to the chronology of (Bergrenn et al. 1995; Cande and Kent, 1995). The white line indicates uncertain age break. Solid black lines are Savitzky–Golay filtered data, grey lines indicate raw data.

Figure S4: Standard deviations of $\delta^{13}C$ and $\delta^{18}O$ data. Box indicates quartiles, black line indicates median, whiskers indicate the remainder of the distribution, diamonds indicate outliers determined through a method that is a function of the inter-quartile range.

Figure S5: Cross-plot of $\delta^{18}O$ v $\delta^{13}C$ indicates no correlation and therefore a minimum of diagenetic alteration. Rho (ϱ) is spearman rank correlation, p is probability value (p-value).

Figure S6: Thin-section photomicrographs of samples: plane polarized light (PPL) (left) and cathodoluminescence (CL) (right). (A&B) Heterogeneous matrix comprised of mud (light brown in PPL) with silt sized detrital quartz and calcite grains (blue and orange luminescence respectively) and foraminifera (arrowed). Stable isotope measurements were derived from this foraminifera-rich material. (B&C) Minor fracture (white arrow) crosscut by a major fracture (red arrow) both cemented by dull blue luminescing calcite. The major fracture is approximately bed parallel, suggesting stylolite cementation. (D&E) Organic matter (dark brown to black in PPL) is bed parallel. Well-developed laminations of quartz-rich (red arrows) and calcite-rich (white arrows) sediment (blue and orange luminescence respectively). Scale bar is 500 μm.

Figure S7: Savitsky-Golay filters of different window lengths for the collected isotopic data. A window-length of 5 was chosen for M1, while a window length of 21 was chosen for M2 and M3 as this window-length best displayed the general trends of the data.

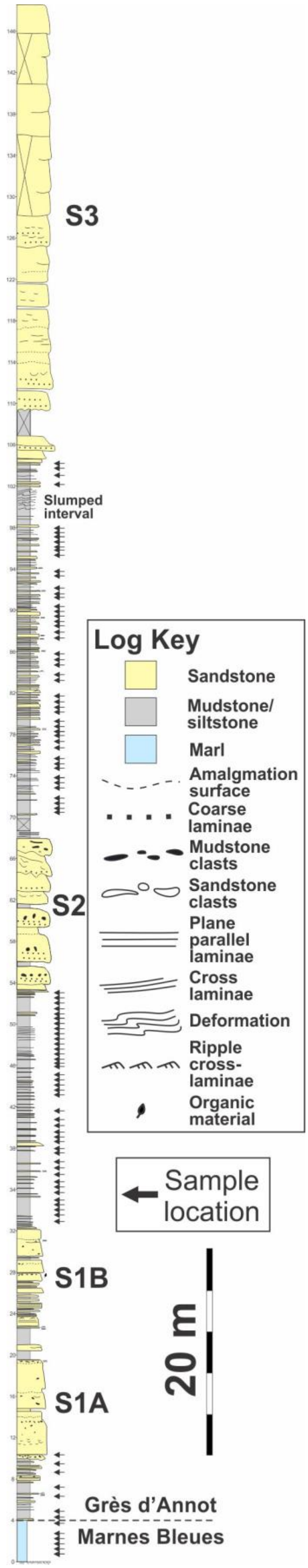
S3
Slumped interval
Log Key
Sandstone
Mudstone/ siltstone
Marl
Amalgmation surface
Coarse laminae
Mudstone clasts
Sandstone clasts
Plane parallel laminae
Cross laminae
Deformation
Ripple cross-laminae
Organic material
S2
Sample location
S1B
20 m
S1A
Grès d'Annot
Marnes Bleues

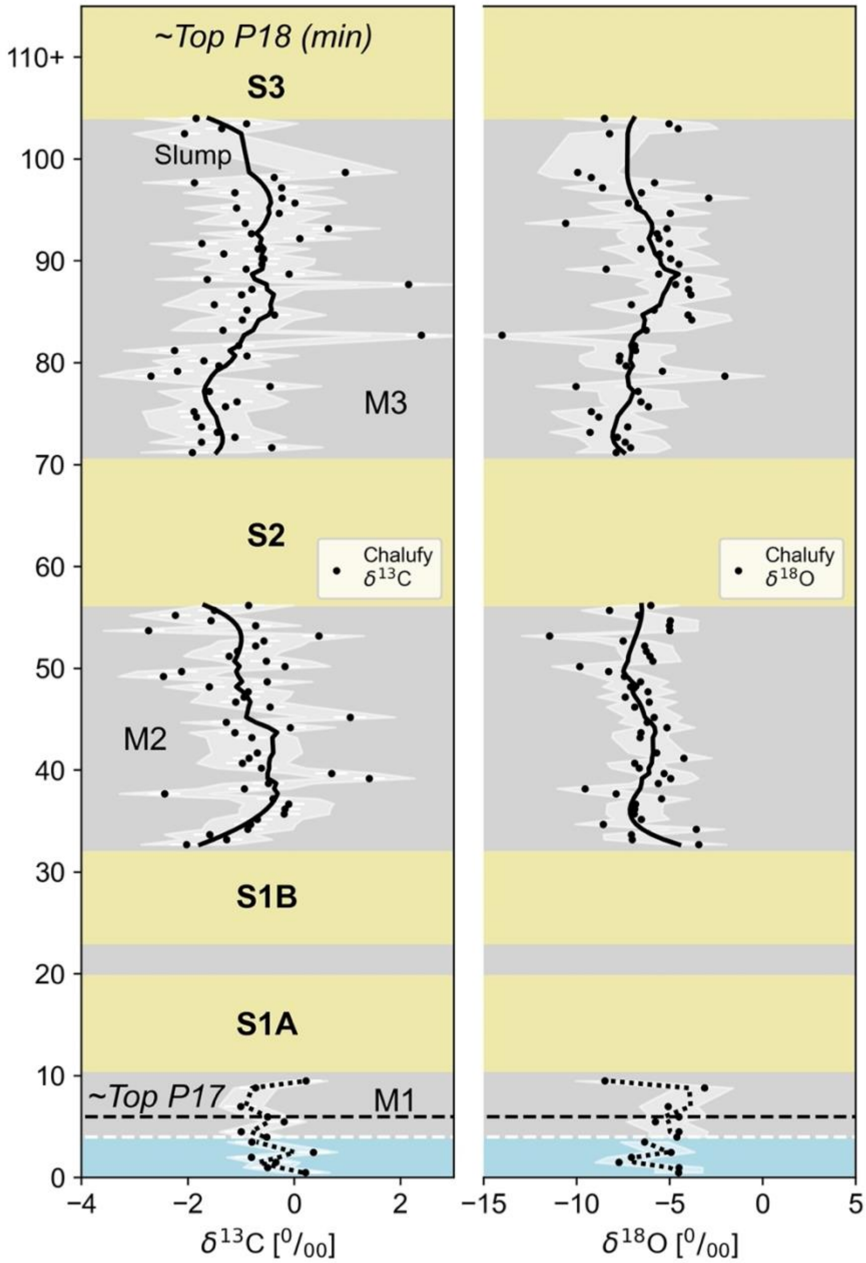
~Top P18 (min)
110+
S3
Slump
100
90
80
M3
70
S2
60
Chalufy
δ^{13}C
Chalufy
δ^{18}O
50
M2
40
30
S1B
20
S1A
10
~Top P17
M1
0
−4
−2
0
2
−15
−10
−5
0
5
δ^{13}C [$^0/_{00}$]
δ^{18}O [$^0/_{00}$]

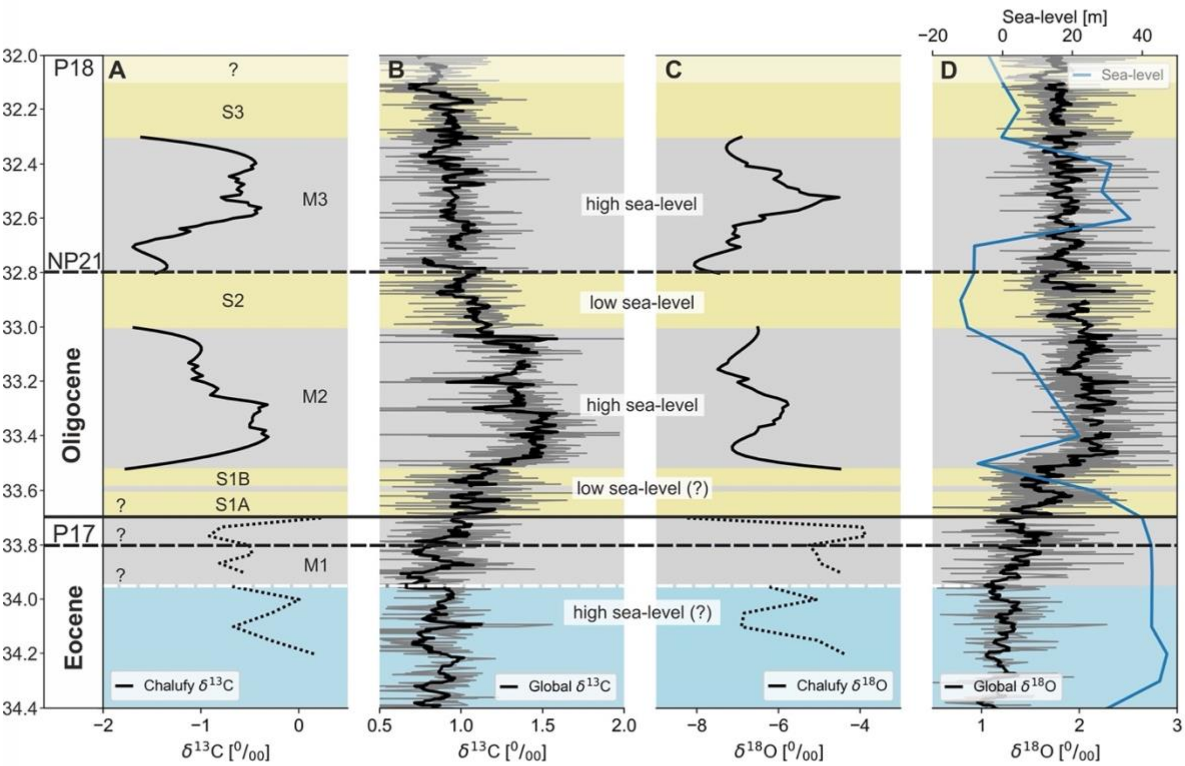

Sea-level [m]
P18
A
B
C
D
S3
M3
NP21
S2
M2
Oligocene
S1B
S1A
P17
M1
Eocene
high sea-level
low sea-level
high sea-level
low sea-level (?)
high sea-level (?)
Sea-level
Chalufy δ13C
Global δ13C
Chalufy δ18O
Global δ18O
δ13C [0/00]
δ13C [0/00]
δ18O [0/00]
δ18O [0/00]

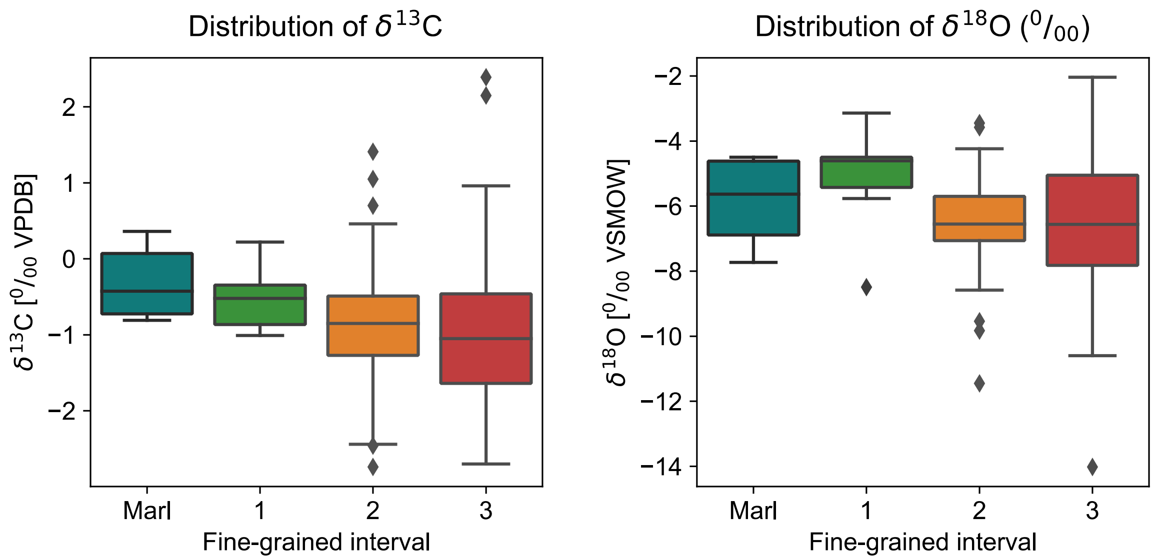

Distribution of δ^{13}C
δ^{13}C [$^0/_{00}$ VPDB]
2
1
0
−1
−2
Marl
1
2
3
Fine-grained interval
Distribution of δ^{18}O ($^0/_{00}$)
δ^{18}O [$^0/_{00}$ VSMOW]
−2
−4
−6
−8
−10
−12
−14
Marl
1
2
3
Fine-grained interval

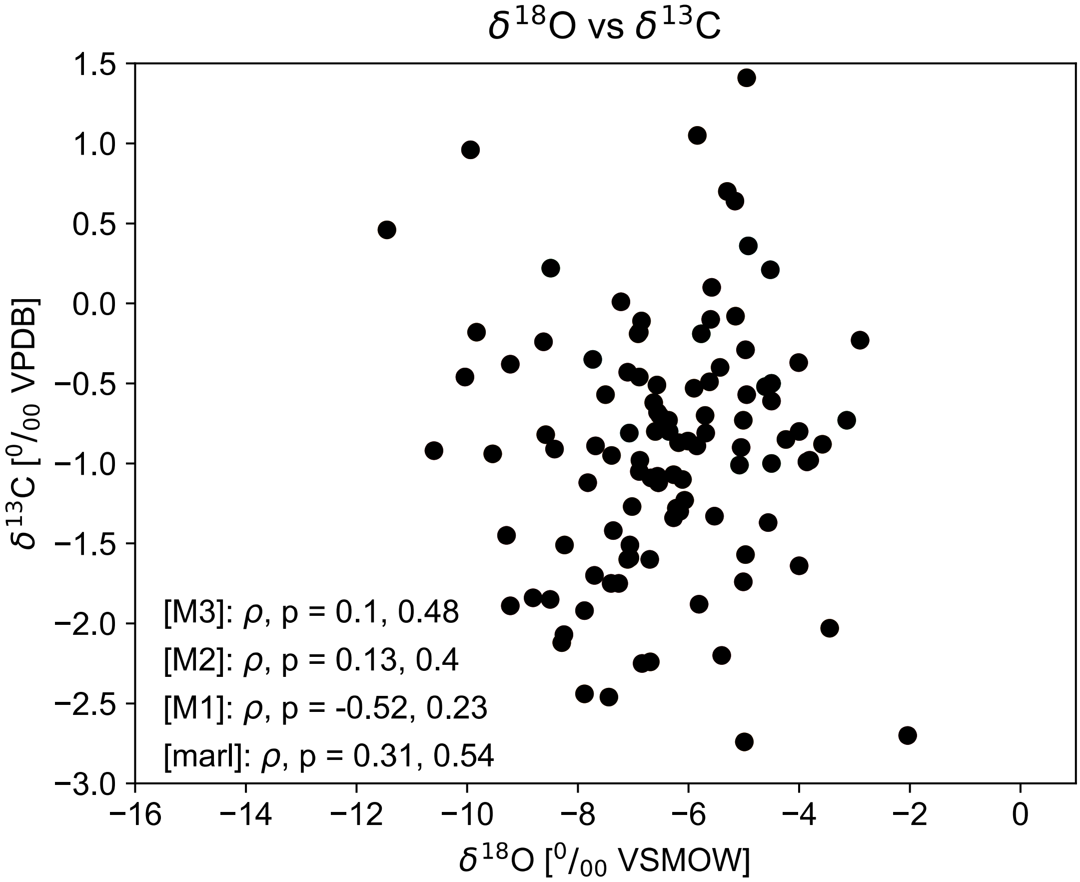

δ^{18}O vs δ^{13}C
1.5
1.0
0.5
0.0
−0.5
−1.0
−1.5
−2.0
−2.5
−3.0
δ^{13}C [$^{0}/_{00}$ VPDB]
[M3]: ρ, p = 0.1, 0.48
[M2]: ρ, p = 0.13, 0.4
[M1]: ρ, p = -0.52, 0.23
[marl]: ρ, p = 0.31, 0.54
−16
−14
−12
−10
−8
−6
−4
−2
0
δ^{18}O [$^{0}/_{00}$ VSMOW]

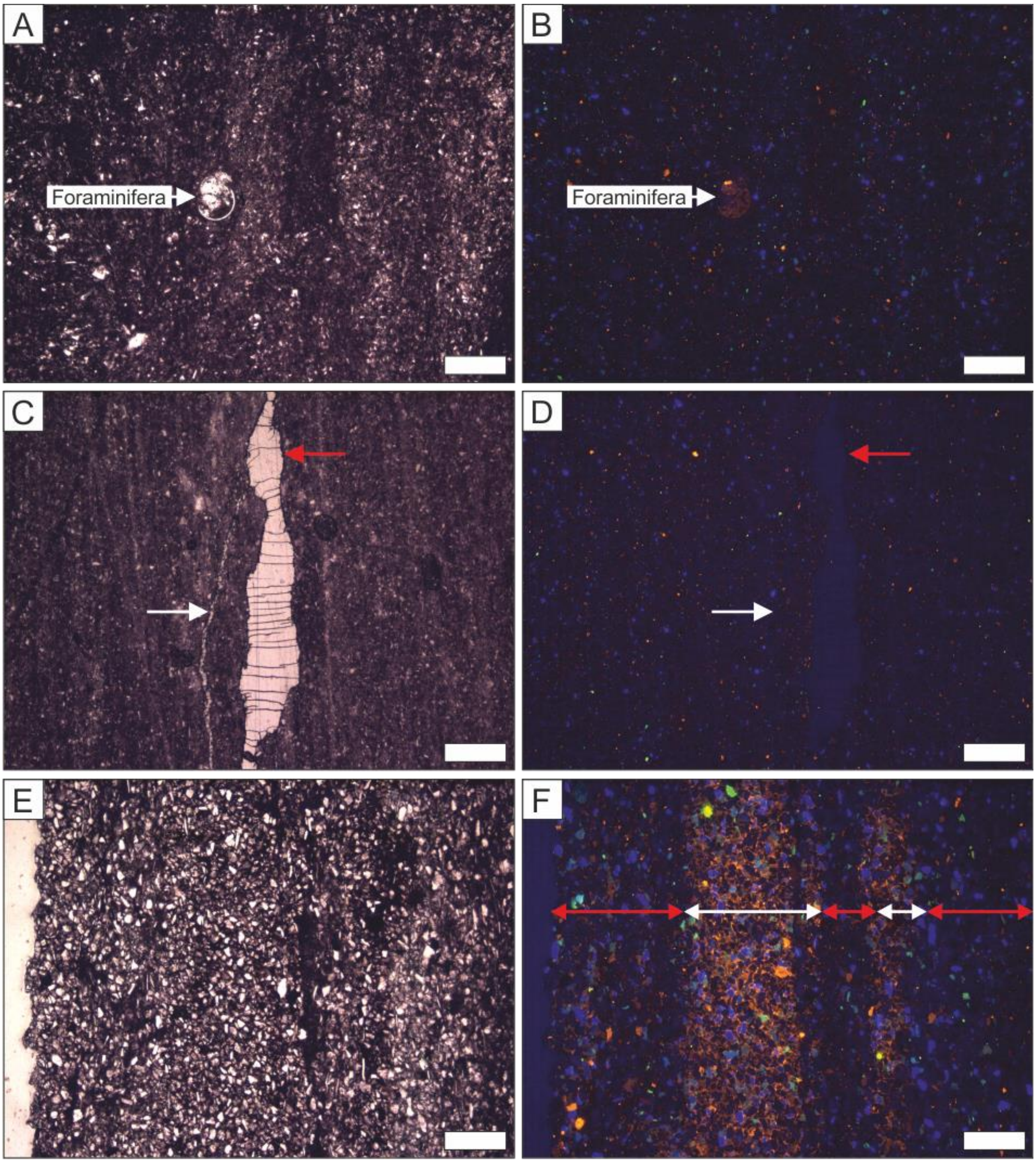
A
Foraminifera
B
Foraminifera
C
D
E
F

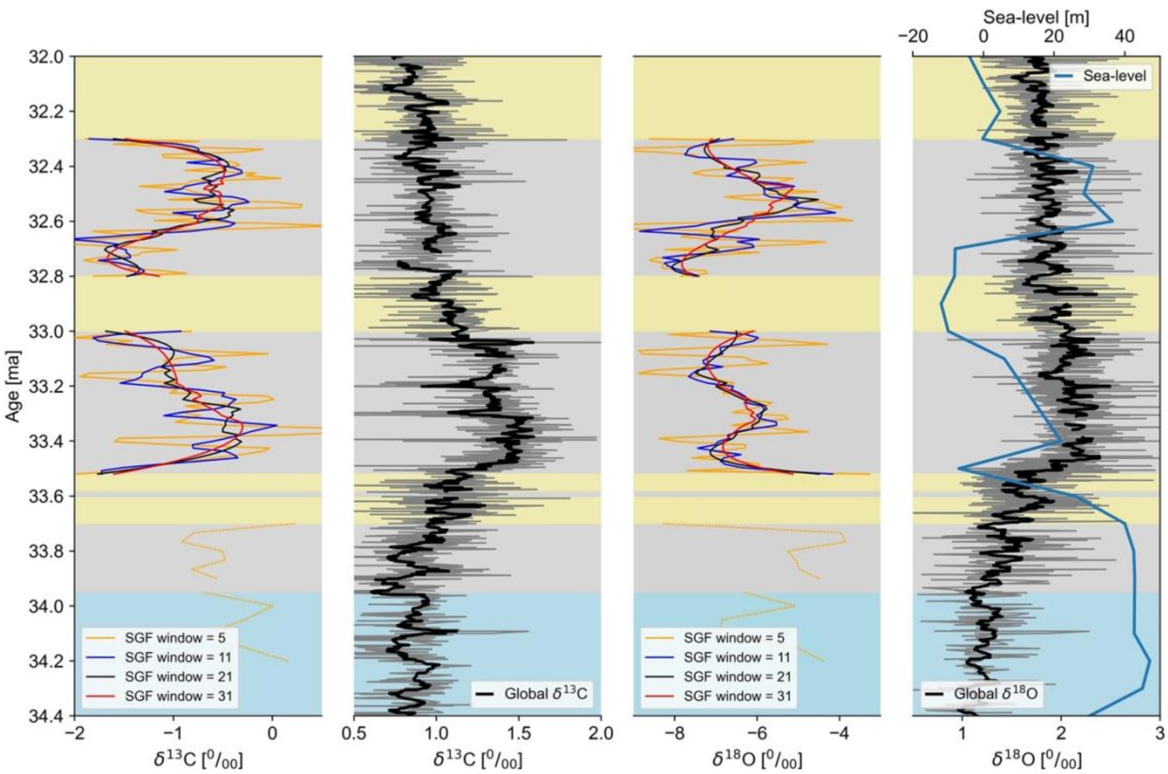

Sea-level [m]
−20
0
20
40
Sea-level
Age [ma]
32.0
32.2
32.4
32.6
32.8
33.0
33.2
33.4
33.6
33.8
34.0
34.2
34.4
SGF window = 5
SGF window = 11
SGF window = 21
SGF window = 31
Global δ^{13}C
Global δ^{18}O
δ^{13}C [$^0/_{00}$]
δ^{13}C [$^0/_{00}$]
δ^{18}O [$^0/_{00}$]
δ^{18}O [$^0/_{00}$]